Stepwise 5′ DNA end-specific resection of DNA breaks by the Mre11-Rad50-Xrs2 and Sae2 nuclease ensemble

Elda Cannavo[a,1], Giordano Reginato[a,b,1], and Petr Cejka[a,b,2]

[a]Institute for Research in Biomedicine, Faculty of Biomedical Sciences, Università della Svizzera italiana, 6500 Bellinzona, Switzerland; and [b]Department of Biology, Institute of Biochemistry, ETH Zurich, 8092 Zurich, Switzerland

Edited by Rodney Rothstein, Columbia University Medical Center, New York, NY, and approved February 4, 2019 (received for review November 27, 2018)

To repair DNA double-strand breaks by homologous recombination, the 5′-terminated DNA strands must first be resected to produce 3′ overhangs. Mre11 from *Saccharomyces cerevisiae* is a 3′ → 5′ exonuclease that is responsible for 5′ end degradation in vivo. Using plasmid-length DNA substrates and purified recombinant proteins, we show that the combined exonuclease and endonuclease activities of recombinant MRX-Sae2 preferentially degrade the 5′-terminated DNA strand, which extends beyond the vicinity of the DNA end. Mechanistically, Rad50 restricts the Mre11 exonuclease in an ATP binding-dependent manner, preventing 3′ end degradation. Phosphorylated Sae2, along with stimulating the MRX endonuclease as shown previously, also overcomes this inhibition to promote the 3′ → 5′ exonuclease of MRX, which requires ATP hydrolysis by Rad50. Our results support a model in which MRX-Sae2 catalyzes 5′-DNA end degradation by stepwise endonucleolytic DNA incisions, followed by exonucleolytic 3′ → 5′ degradation of the individual DNA fragments. This model explains how both exonuclease and endonuclease activities of Mre11 functionally integrate within the MRX-Sae2 ensemble to resect 5′-terminated DNA.

DNA | nuclease | homologous recombination | Mre11 | DNA end resection

DNA double-strand breaks (DSBs) represent one of the most cytotoxic forms of DNA damage (1). Eukaryotic cells possess two main pathways for DSB repair, nonhomologous end-joining (NHEJ) and homologous recombination (HR) (2). NHEJ is a fast, cell-cycle independent but inaccurate process that restores DNA integrity by ligating the broken DNA molecules (3). In contrast, HR is a template-directed pathway that restores DNA integrity in a mostly accurate manner by using DNA information stored in a homologous DNA template (4). In contrast to NHEJ, the DNA ends in HR must be extensively processed to reveal 3′-terminated ssDNA overhangs in a process termed 5′ DNA end resection (5). The resulting 3′ overhangs are necessary for the downstream steps of the HR pathway to search for a homologous sequence and prime DNA synthesis (2).

The Mre11-Rad50-Xrs2/NBS1 complex (MRX in *Saccharomyces cerevisiae*, MRN in humans) recognizes, signals, and initiates the repair of DSBs (6–9). Specifically, the MRX/MRN complex has key roles in DNA end resection. These functions include a nucleolytic role of Mre11 in the vicinity of the DSB, termed short-range resection, as well as structural functions to promote the recruitment of Dna2 and Exo1 nucleases that function further downstream and catalyze long-range resection (10–16). The Mre11 nuclease in *S. cerevisiae* is particularly important when DNA ends are bound by Ku or Spo11 or contain secondary DNA structures (17–22). The Mre11 nuclease and Sae2/CtIP/Ctp1 likely are more important for resection in other organisms, including fission yeast and humans (23, 24).

The involvement of the Mre11 nuclease in 5′ DNA end resection had been puzzling, because Mre11 was first characterized as a 3′ → 5′ exonuclease, which has the opposite polarity to that required for resection (25). Physical assays instead clearly demonstrated that in vivo Mre11 is responsible for degradation of the 5′-terminated DNA strand (13). The degradation of the 5′ strand can proceed up to approximately 300 nt in length, which has been observed in both vegetative and meiotic cells, particularly in the absence of the long-range resection pathways (13, 26). Resection of DNA ends by the Mre11 nuclease is likely initiated by an endonucleolytic DNA cleavage of the 5′ strand. This mode of resection was first established in yeast meiotic cells, in which the breaks are formed by Spo11, which remains covalently bound to the 5′ end. Spo11 was found attached to short DNA fragments, indicative of endonucleolytic cleavage during the subsequent processing (21, 27, 28). In vegetative cells, the Mre11 nuclease helps remove Ku and stalled topoisomerases, demonstrating an important yet nonessential function of the Mre11 nuclease in vegetative cells as well (20, 23, 29–31). Using a reconstituted system, we and others have shown that phosphorylated Sae2 (pSae2), or pCtIP in humans, promotes the Mre11 nuclease within the MRX/MRN complex to cleave the 5′-terminated DNA strand endonucleolytically adjacent to protein-bound DSBs. The MRX-pSae2 ensemble could cleave DNA ∼15–20 nt away from a streptavidin block and up to ∼35–40 nt away from a Ku-bound DSB, in accordance with the larger DNA-binding site size of Ku (17, 18, 32–34). However, the DNA clipping next to a DSB-bound protein block cannot explain the capacity of MRX to resect 5′-terminated DNA further away from the break, as observed in cells (13, 26).

The Mre11 endonuclease function integrates with the ATPase of Rad50 (11, 32–35). In contrast, Mre11 is a 3′→5′ exonuclease on its own (11), and the interplay of the Mre11 exonuclease with Rad50 and Sae2 has not been defined to date. Here we show that Rad50, in the presence of ATP, strongly restricts the exonuclease of Mre11. These results show that the 3′→5′ exonuclease activity of the MRX complex is very limited, explaining why the 3′ end is protected. pSae2 can partially overcome this inhibition, which

Significance

The Mre11-Rad50-Xrs2 (MRX)-Sae2 complex has key functions in initiating the repair of DNA double-strand breaks by homologous recombination. Using purified recombinant proteins, we demonstrate how ATP binding and hydrolysis by the Rad50 subunit regulate the nuclease activities of Mre11. We reconstitute a reaction wherein the MRX-Sae2 ensemble preferentially degrades the 5′-terminated DNA strands at DNA break sites up to several hundred nucleotides in length. This polarity of DNA end processing is required for homologous recombination. Our experiments help explain how MRX-Sae2 and their homologs contribute to the maintenance of genome stability.

Author contributions: P.C. designed research; E.C. and G.R. performed research; E.C., G.R., and P.C. analyzed data; and E.C., G.R., and P.C. wrote the paper.

The authors declare no conflict of interest.

This article is a PNAS Direct Submission.

[1]E.C. and G.R. contributed equally to this work.

[2]To whom correspondence should be addressed. Email: petr.cejka@irb.usi.ch.

This article contains supporting information online at www.pnas.org/lookup/suppl/doi:10.1073/pnas.1820157116/-/DCSupplemental.

requires ATP hydrolysis by Rad50. However, because pSae2 also promotes the endonuclease of MRX as shown previously (33), the exonuclease and endonuclease reactions of MRX-pSae2 likely compete with each other. Using plasmid-length DNA substrates, we found that the combined activities of the MRX-pSae2 ensemble preferentially degrade the 5′-terminated DNA strand beyond the immediate vicinity of the DNA end. These findings strongly support a model in which the 5′-terminated DNA strand near a DSB is degraded by stepwise clipping by MRX-pSae2 and does not require a separate protein block. In this model, the 3′→5′ exonuclease activity of Mre11, also controlled by Rad50 and pSae2, is limited to degrade the short DNA fragments between the endonucleolytic cleavage sites. Taken together, these results define a mechanism that explains the preferential 5′ DNA end degradation by the MRX-pSae2 complex at DSBs.

Results

MRX and pSae2 Preferentially Degrade 5′ Terminated DNA Strands of Blunt-Ended Plasmid-Length DNA Substrates. To study DNA end resection by MRX and pSae2, we prepared individual components of the MRX complex including Mre11, Rad50, and Xrs2, as well as Mre11-Rad50 (MR), Mre11-Xrs2 (MX), and Mre11-Rad50-Xrs2 (MRX) complexes (Fig. 1*A*). Recombinant MRX and pSae2 clip the 5′-terminated DNA strand next to Ku- or streptavidin-bound DSBs (17, 18, 33). To study DNA processing by MRX beyond the immediate vicinity of the DNA end, we

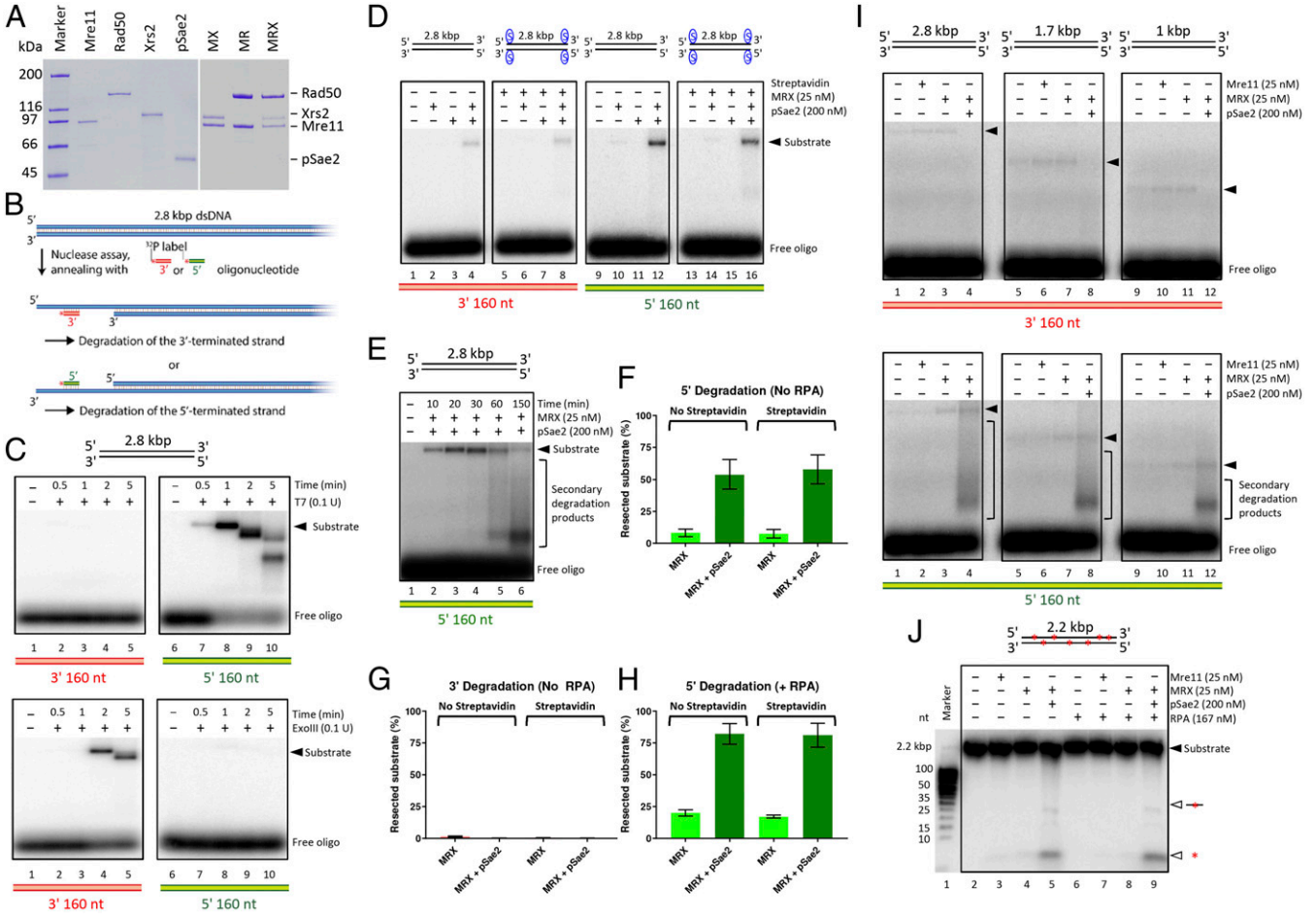

Fig. 1. MRX and pSae2 preferentially degrade 5′ terminated DNA strands of blunt-ended plasmid-length DNA substrates. (*A*) Overview of selected proteins used in this study. MR, Mre11-Rad50; MRX, Mre11-Rad50-Xrs2; MX, Mre11-Xrs2. The proteins were separated by electrophoresis in 4–15% gradient polyacrylamide gel and then stained with Coomassie blue. (*B*) A scheme of the annealing assay that uses radiolabeled oligonucleotides to detect ssDNA on resection of plasmid-length dsDNA. Oligonucleotides complementary to either the 5′ or 3′ strand at the position away from the DNA end indicated in each panel were used. (*C*) Kinetics of blunt-ended 2.8-kbp-long dsDNA substrate degradation by T7 exonuclease (*Top*) or ExoIII exonuclease (*Bottom*) detected by the annealing assay. Oligonucleotides complementary to a region approximately 160 nt away from the DNA end were used to detect 5′ (5′_OligoA) and 3′ (3′_OligoA) end degradation. (*D*) Blunt-ended, 2.8-kbp-long dsDNA with free or streptavidin-blocked DNA ends was incubated with MRX and/or pSae2 for 25 min. The products were annealed with oligonucleotides detecting the resection of the 3′-terminated (*Left*) or 5′-terminated (*Right*) DNA strand. A representative experiment is shown. The contrast of the image was enhanced to facilitate visualization of the annealing products. (*E*) Kinetics of DNA degradation by MRX with pSae2. DNA degradation was analyzed by annealing of the reaction products with 5′_OligoA, which detects degradation of the 5′-terminated DNA strand. The solid triangle represents the positions of the full-length DNA substrate and the initial resection products. Extended resection products and products resulting from secondary cleavage are indicated in brackets. A representative experiment is shown. (*F*) Quantitation of 5′ strand degradation in experiments similar to those shown in *D* but on 2.5 h of reaction time. $n = 4$. Error bars represent SEM. (*G*) Quantitation of 3′ end degradation in experiments similar to those shown in *D* but on 2.5 h of reaction time. $n = 4$. Error bars represent SEM. (*H*) Quantitation of 5′ degradation in experiments similar to those shown in *D* but on 2.5 h of reaction time, performed in the presence of RPA. $n = 4$. Error bars represent SEM. (*I*) Reactions as in *D* but with dsDNA substrates of different lengths, incubated for 2.5 h. The solid triangles represent the positions of the full-length DNA substrate and the initial resection products. Extended resection and products resulting from secondary cleavage are indicated in brackets. Representative experiments are shown. (*J*) Degradation of randomly labeled 2.2-kbp-long DNA by Mre11, MRX, and pSae2. The reaction products were analyzed on 15% denaturing gel.

used blunt-ended plasmid-length DNA substrates. We monitored resection by the annealing of radiolabeled oligonucleotides that were complementary to either the top (5′-terminated) or the bottom (3′-terminated) DNA strand at a position approximately 160 nt away from the end (Fig. 1*B*). Resection of the 5′-terminated DNA strand allows annealing of the top strand probe, while the resected 3′-terminated strand anneals with the bottom strand probe. As expected, T7 exonuclease gave a signal with the top strand probe indicating resection of the 5′-terminated DNA strand (Fig. 1*C*, *Top*), consistent with its 5′→3′ polarity of DNA degradation. In contrast, the *Escherichia coli*'s 3′→5′ exonuclease ExoIII produced a strong signal only with the 3′-specific probe (Fig. 1*C*, *Bottom*).

We next monitored DNA degradation by MRX with or without pSae2. Unexpectedly, we found that the MRX-pSae2 ensemble on its own preferentially degraded the 5′-terminated DNA strand, as the degradation of the 3′-terminated strand was much weaker after 25 min of reaction (Fig. 1*D*). The 5′ strand degradation by MRX was strongly stimulated by pSae2, as very little signal was detected in assays containing MRX alone, and no signal was detected with pSae2 alone (Fig. 1*D*). Kinetic experiments revealed that the fraction of the resected 5′-terminated strand increased with time (Fig. 1*E*). The 3′ overhang was then cleaved off in a secondary event, giving rise to a faster-migrating species (Fig. 1*E*), in agreement with the known capacity of recombinant MRX to cleave at junctions of ssDNA and dsDNA and at secondary DNA structures (11). After 2.5 h, more than 50% of 5′ DNA ends were resected beyond 160 nt by MRX-pSae2 (Fig. 1*F*). In contrast, degradation of the 3′-terminated strand was much weaker and became undetectable after 2.5 h (Fig. 1*G* and *SI Appendix*, Fig. S1 *A* and *B*). Of note, the efficacy of DNA degradation was unaffected by streptavidin blocks at the DSBs (Fig. 1 *D*, *F*, and *G* and *SI Appendix*, Fig. S1*C*). These results demonstrate that a separate protein block is not necessary for the resection capacity of the MRX-pSae2 ensemble, and that the degradation involves endonucleolytic DNA cleavage. The reaction was promoted by the ssDNA binding replication protein A (RPA), which resulted in >75% 5′ strand degradation at 2.5 h (Fig. 1*H* and *SI Appendix*, Fig. S1*D*). The stimulatory function of RPA is in agreement with the idea that RPA may serve as a protein block to direct the MRX-pSae2 endonuclease (17, 18). Also with RPA, the degradation of the 3′-terminated strand was much less efficient than the degradation of the 5′ strand (*SI Appendix*, Fig. S1 *D* and *E*). The preferential degradation of the 5′ strand by MRX-pSae2 was not affected by the length of the DNA substrate (Fig. 1*I*). We observed a notable degradation of the 5′ strand at ∼125 and ∼160 nt, but not at ∼280 nt, away from the end (*SI Appendix*, Fig. S1*F*). Finally, pSae2 likewise stimulated DNA resection by MRX in reactions monitored by total DNA staining with GelRed (*SI Appendix*, Fig. S1 *G* and *H*).

The preferential degradation of the 5′-terminated DNA strand cannot result from exonucleolytic DNA degradation, because the Mre11 exonuclease has the opposite, 3′→5′ polarity (11). Rather, the results suggest a model in which the 5′-end degradation stems from a stepwise endonucleolytic cleavage, which is more efficient than the competing exonucleolytic degradation of the 3′ end. The 3′→5′ exonuclease of Mre11 would then be limited to degradation of the short DNA fragments between the endonucleolytic cleavage sites. To test this hypothesis, we prepared a randomly labeled blunt-ended 2.2-kbp-long dsDNA molecule and subjected to MRX and pSae2. We observed DNA fragments of ∼25 nt in length as well as mononucleotide products (Fig. 1*J*), in agreement with the above model. Our experiments in summary demonstrate that the 3′→5′ MRX exonuclease alone cannot efficiently resect long lengths of blunt-ended DNA. When together with pSae2, the ensemble preferentially resects DSBs with a 5′ polarity that is required for HR rather than degrading the 3′-terminated DNA strand. This reconstituted 5′ DNA degradation can proceed beyond the vicinity (>160 nt) of the DNA end, as observed in vivo (13).

Rad50 Inhibits the Mre11 Exonuclease in an ATP-Binding–Dependent Manner. To understand the mechanisms underlying the preferential 5′ DNA degradation by MRX-pSae2, we set out to better define the regulation of the nuclease activities of the MRX-pSae2 ensemble. It has been established that the Mre11 endonuclease generally requires Rad50 and pSae2 but can function as an exonuclease on its own (11, 33, 36). Whether Mre11 exonuclease activity is regulated within the MRX-Sae2 complex has not been defined. To monitor the Mre11 exonuclease, we next used an oligonucleotide-based dsDNA substrate (Fig. 2*A*). The exonucleolytic degradation of the top DNA strand was blocked by phosphorothioate bonds at the 3′ end. The bottom DNA strand was ^{32}P-labeled at the 5′ end, which allowed us to monitor its degradation in the 3′→5′ direction (Fig. 2*A*). As established, Mre11 is a 3′→5′ exonuclease (*SI Appendix*, Fig. S2*A*) (11). The exonuclease of Mre11 was not affected by ATP or the nonhydrolyzable analog ATP-γ-S (*SI Appendix*, Fig. S2 *A* and *B*). We also found that the observed nucleolytic activity was intrinsic to Mre11, because the Mre11 125–126 HD-LV mutant (Mre11 ND) with a disrupted nuclease active site did not show any activity (*SI Appendix*, Fig. S2 *C* and *D*) (37). Under our conditions, the exonuclease of Mre11 was not notably affected by Xrs2 independent of the nucleotide cofactor (*SI Appendix*, Fig. S2 *E* and *F*).

We next supplemented the Mre11 nuclease reactions with various concentrations of Rad50 (Fig. 2*B*). We observed that Rad50 moderately inhibited Mre11 exonuclease in a concentration-dependent manner without ATP, but its inhibitory effect was much more pronounced in reactions containing ATP and especially with ATP-γ-S (Fig. 2 *C* and *D*) (11). Quantitation of these experiments revealed that 25 nM Mre11 alone degraded ∼50% of the bottom DNA strand within 30 min. With ATP, an equimolar concentration of Rad50 (25 nM) inhibited the Mre11 exonuclease by ∼2.5-fold; with ATP-γ-S, the inhibition was ∼20-fold (Fig. 2 *C* and *D*). In contrast, ADP inhibited Mre11 and Rad50 only moderately (*SI Appendix*, Fig. S2 *G* and *H*). AMP-PNP, another nonhydrolyzable ATP analog, inhibited MR similarly to ATP-γ-S and comparably to ADP·vanadate, a transition state analog (*SI Appendix*, Fig. S2 *G* and *H*) (38). These results suggest that ATP binding, but not ATP hydrolysis, by Rad50 limits the Mre11 exonuclease.

To further confirm this conclusion, we expressed and purified the Rad50 K40A mutant (Rad50 KA hereinafter), which is believed to be impaired in ATP binding and hydrolysis (35) (Fig. 2*B*). As wild-type Rad50, Rad50 KA very weakly inhibited the Mre11 exonuclease without ATP; however, in contrast to wild-type Rad50, Mre11 exonuclease together with Rad50 KA was not strongly affected by the nucleotide cofactor (Fig. 2 *E* and *F*). Furthermore, ATP (and ATP-γ-S) inhibited the exonuclease of the MR and MRX complexes, but not the exonuclease of the MX complex, confirming the specific role of Rad50·ATP in Mre11 exonuclease inhibition (*SI Appendix*, Fig. S2*I*). This inhibitory function of Rad50 was apparent in reaction buffers with various magnesium and manganese concentrations (compare *SI Appendix*, Fig. S2*I* with Fig. 2 *C* and *D*). The nuclease activity in reactions with Mre11 and Rad50 was dependent on the integrity of the nuclease motif of Mre11, as expected (*SI Appendix*, Fig. S2*J*). Collectively, these experiments establish that Rad50, in complex with Mre11, limits its exonuclease activity in an ATP binding-dependent manner. The limited 3′→5′ exonuclease capacity of MRX under physiological conditions in the presence of ATP likely explains why the 3′ end at DSBs in vivo is largely protected from degradation.

pSae2 Promotes Mre11 Exonuclease When Rad50 Is Present. We next set out to determine whether pSae2 regulates the exonuclease activity of the MRX complex. We observed that in the presence of

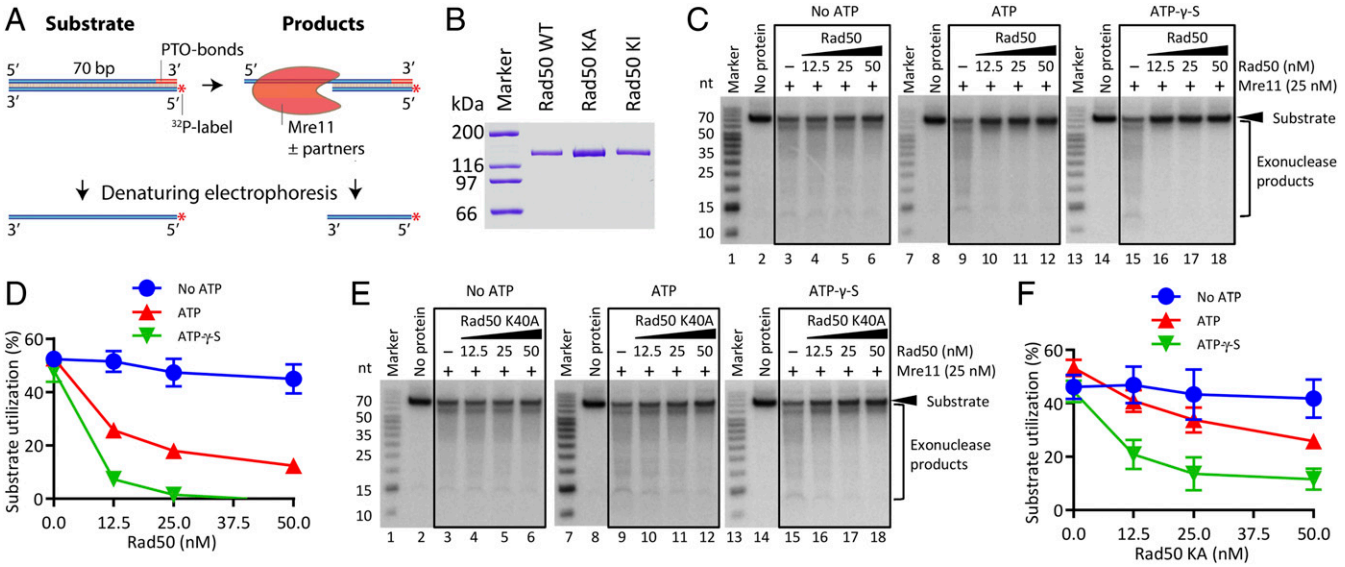

Fig. 2. Rad50 inhibits the exonuclease of Mre11 in an ATP-binding–dependent manner. (*A*) Scheme of the 5′ end-labeled DNA substrate used to monitor the 3′→5′ exonuclease of Mre11 and its partners. Phosphorothioate (PTO) bonds prevent the 3′→5′ exonucleolytic degradation of the top DNA strand. (*B*) Coomassie blue-stained polyacrylamide gel (10%) of the indicated Rad50 variants. (*C*) DNA degradation by Mre11 in the presence of various concentrations of Rad50 without ATP, with ATP, or with nonhydrolyzable ATP-γ-S. The reaction buffer contained 5 mM Mn^{2+} and 0.1 mM Mg^{2+}. (*D*) Quantitation of experiments such as in *C*. $n = 3$. Error bars represent SEM. (*E*) Experiments as in *C* showing DNA degradation by Mre11 but with various concentrations of the ATP binding-impaired Rad50 K40A (Rad50 KA) variant. (*F*) Quantitation of experiments such as in *E*. $n \geq 3$. Error bars represent SEM.

ATP, pSae2 clearly promoted the exonuclease of MRX (Fig. 3*A*) and the MR complex (Fig. 3 *B* and *C*). The nuclease required the integrity of the Mre11 nuclease active site, and pSae2 alone did not support DNA degradation, confirming that the nuclease is intrinsic to Mre11 (Fig. 3*A*). Sae2 is phosphorylated by multiple kinases, including cyclin-dependent kinase (CDK) and Mec1/Tel1, in a cell cycle- and DNA damage-dependent manner (36, 39). Sae2 phosphorylation is essential for its stimulatory effect on the MRX endonuclease near protein-blocked ends (33, 36). In exonuclease assays, pSae2, in contrast to lambda phosphatase-treated Sae2 (Sae2-λ), stimulated DNA degradation by the MR complex (Fig. 3 *B* and *C* and *SI Appendix*, Fig. S3*A*). pSae2 stimulated DNA degradation by MR, as assayed by overall substrate utilization, but the effect was more pronounced when we quantitated the appearance of small DNA degradation products <~15 nt long (compare Fig. 3*C* and *SI Appendix*, Fig. S3*A*). The CDK site of pSae2 at S267 specifically needs to be phosphorylated, as the nonphosphorylatable pSae2 S267A (pSae2 SA) mutant was inefficient in MR stimulation (Fig. 3 *D* and *E* and *SI Appendix*, Fig. S3*B*) (36, 39). In contrast, the phosphomimetic pSae2 S267E (pSae2 SE) variant stimulated the exonuclease of MR by ~2.6-fold, compared with ~3.3-fold stimulation by wild-type Sae2 (Fig. 3 *D* and *E* and *SI Appendix*, Fig. S3*B*).

We next examined the MX complex. As above, we observed that Rad50 inhibited the MX exonuclease (Fig. 3 *F* and *G*; all reactions were carried out with ATP). pSae2, but not Sae2-λ, was able to overcome this inhibition (Fig. 3 *F* and *G*). In contrast to MR or MRX, under our conditions, pSae2 did not promote the exonuclease of Mre11 alone, showing that Rad50 is needed for the observed stimulatory effect (*SI Appendix*, Fig. S3 *C*–*E*). Our observation that pSae2 similarly stimulated the MR and MRX complexes shows that Xrs2 does not play an essential role in mediating the stimulatory effect of pSae2 on the exonuclease activity of MRX, although it may have a stimulatory function under other conditions (18).

Although the kinetic experiments with oligonucleotide-based substrates showed gradual DNA degradation from the 3′ end, indicating that the exonuclease activity of Mre11 was likely stimulated (Fig. 3*B*), it is possible that some of the DNA degradation occurred through an endonucleolytic mechanism. To differentiate between these two possibilities, we next used a plasmid-length DNA substrate. Because blunt-ended DNA was not efficiently degraded by the 3′→5′ exonuclease of MRX, we used DNA with ~28-nt-long 5′ overhangs, which provides a good substrate for the MRX exonuclease. Indeed, using this substrate, we detected 3′-end degradation by MRX (Fig. 3*H*). In agreement with our observations that pSae2 promotes the 3′→5′ exonuclease of MRX, pSae2, but not Sae2-λ, stimulated the degradation of the 3′-terminated recessed DNA strand by ~2.4-fold. The degradation was dependent on the nuclease of Mre11 and required ATP (Fig. 3*H*). The same results were obtained in experiments in which we varied the pSae2 concentration (approximately twofold stimulation with 40 nM Sae2; Fig. 3*I*) or in which we annealed labeled probes complementary to various distances from the end (*SI Appendix*, Fig. S3*F*), as well as in a kinetic assay (*SI Appendix*, Fig. S3*G*). In contrast to MRX, pSae2 did not stimulate the nuclease of Mre11 without Rad50 (*SI Appendix*, Fig. S3*H*). We note that pSae2 also promoted the degradation of the 5′-terminated DNA strand (Fig. 3*I*), but the efficiency of the 5′-overhanged substrate resection by MRX-pSae2 was much lower than that of the blunt-ended substrate (compare Fig. 3*I* and Fig. 1*E*).

We next used a similar substrate as shown in Fig. 2*A*, but labeled the bottom DNA strand at the 3′ end, and repeated the nuclease reactions with Mre11, Rad50, pSae2, and ATP (Fig. 4*A*). In this case, the DNA degradation resulted in a single detectable product of a very small size, confirming the 3′→5′ exonucleolytic mode of DNA degradation starting at the 3′ end. Interestingly, this experiment revealed that Rad50 inhibited Mre11 already during the cleavage of the first terminal nucleotide from the 3′ end bearing the ^{32}P-label (Fig. 4 *A* and *B*). This result was also obtained when Rad50 was titrated into reactions containing Mre11 (*SI Appendix*, Fig. S4 *A* and *B*), irrespective of the relative manganese acetate (Mn^{2+}) and magnesium acetate (Mg^{2+}) concentrations (*SI Appendix*, Fig. S4 *C* and *D*), and also when Rad50 was added to the MX complex (*SI Appendix*, Fig. S4 *E*

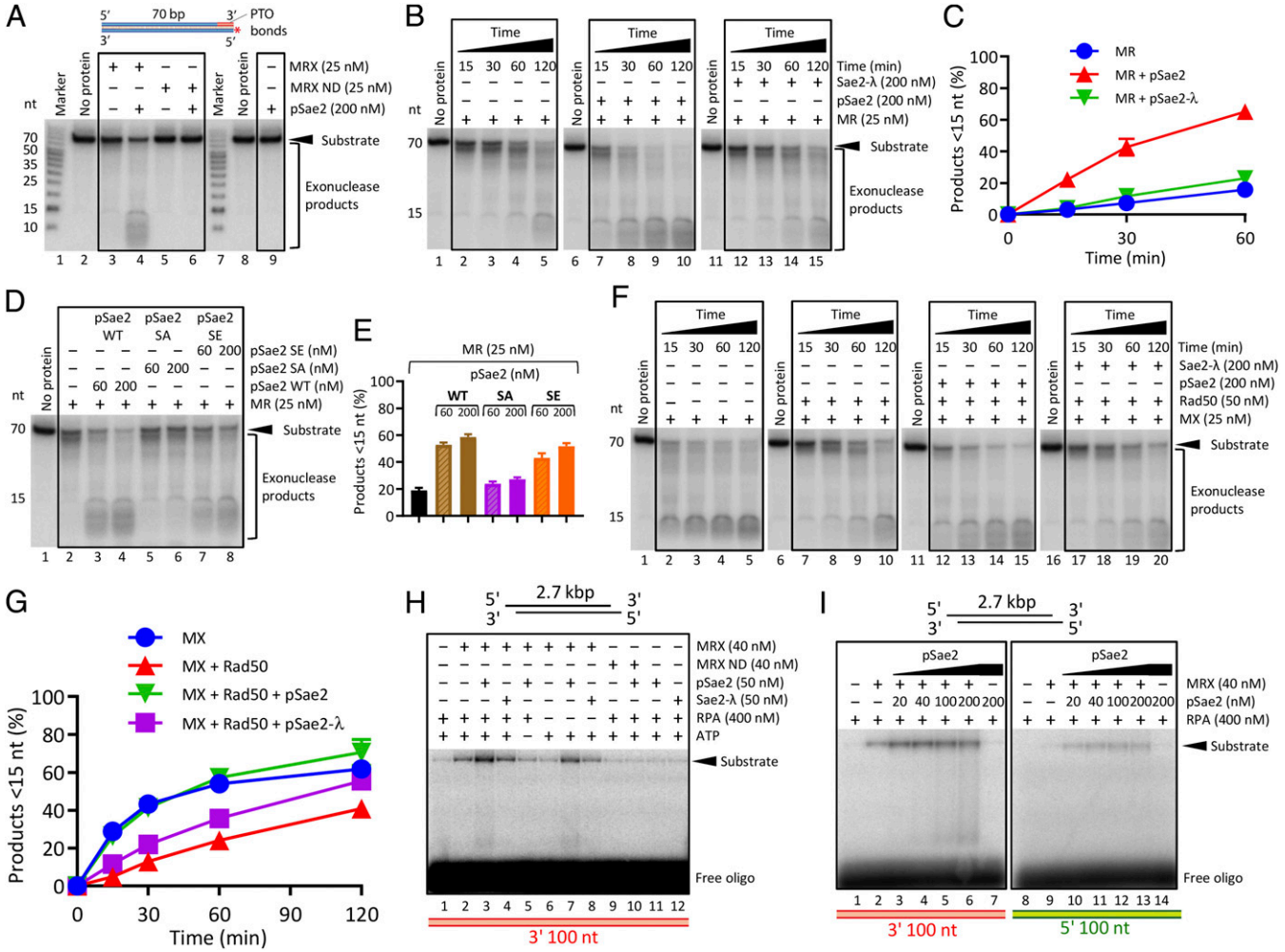

Fig. 3. pSae2 promotes the exonuclease of Mre11 when Rad50 is present. (*A*) Degradation of 5′ end-labeled DNA substrate (Fig. 2*A*) by MRX, nuclease-deficient Mre11 (125-126 HD-LV)-Rad50-Xrs2 (MRX ND), and pSae2, as indicated, in the presence of ATP, 5 mM Mg^{2+}, and 1 mM Mn^{2+}. (*B*) Kinetics of DNA degradation by the MR complex and the effects of pSae2 and Sae2-λ. The reaction buffer contained ATP, 5 mM Mg^{2+}, and 1 mM Mn^{2+}. The substrate was as in *A*. (*C*) Quantitation of experiments such as in *B*. $n \geq 3$. Error bars represent SEM. (*D*) DNA degradation by MR in reactions supplemented with wild-type pSae2, pSae2 S267A (pSae2 SA, nonphosphorylatable at S267 but phosphorylated at other residues), or phospho-mimicking pSae2 S267E (pSae2 SE, phosphomimicking at S267 and phosphorylated at other residues). The reaction buffer contained ATP, 5 mM Mg^{2+}, and 1 mM Mn^{2+}. The substrate was as in *A*. (*E*) Quantitation of experiments such as in *D*. $n = 3$. Error bars represent SEM. (*F*) Kinetics of DNA degradation by MX, Rad50, and pSae2 or Sae2-λ, as indicated. The reaction buffer contained ATP, 5 mM Mg^{2+}, and 1 mM Mn^{2+}. The substrate was as in *A*. (*G*) Quantitation of experiments such as in *F*. $n = 3$. Error bars represent SEM. (*H*) Degradation of 5′ tailed 2.7-kbp-long DNA by MRX, pSae2, and variants, as indicated. The reaction products were annealed with an oligonucleotide that detects the degradation of the 3′-terminated DNA strand approximately 100 nt away from the end (3′_OligoA). A representative experiment is shown. (*I*) Degradation of 5′ tailed DNA substrate by MRX and various concentrations of pSae2, as indicated. The degradation of 5′ and 3′ terminated strands was monitored (3′_OligoA and 5′_OligoA). Representative experiments are shown.

and *F*). In contrast, pSae2 did not affect the first cleavage event (Fig. 4*A*, compare lanes 3 and 4 and lanes 7 and 8, and *B*), in agreement with previously reported data (33). Thus, pSae2 promotes the exonucleolytic degradation of DNA by MR downstream of the first cut. We obtained similar results in the presence of Xrs2 (Fig. 4 *C* and *D*). Collectively, these results suggest that pSae2 promotes Mre11 exonuclease when Rad50 is present.

The Stimulation of Mre11 Exonuclease by pSae2 Requires ATP Hydrolysis by Rad50. To determine whether the stimulation of Mre11 exonuclease by pSae2 requires ATP hydrolysis by Rad50, we compared the effect of pSae2 on the exonuclease of MRX in reactions with various nucleotide cofactors and their analogs. pSae2 did not notably affect the exonuclease of MRX in reactions without ATP (Fig. 5 *A* and *B*) or with ADP (*SI Appendix*, Fig. S5 *A*–*C*), and could not rescue the inhibition of the MRX exonuclease with nonhydrolyzable ATP-γ-S (Fig. 5 *C* and *D*), AMP-PNP or ADP-vanadate (*SI Appendix*, Fig. S5 *A*–*C*). Strikingly, pSae2 promoted MRX activity only in the presence of ATP (Fig. 5 *E* and *F*), or when ADP was coupled with the ATP regeneration system consisting of pyruvate kinase and phosphoenolpyruvate (*SI Appendix*, Fig. S5 *A*–*C*). As above, we note that pSae2 stimulated overall substrate degradation only moderately, while it promoted the extent to which DNA was degraded (*SI Appendix*, Fig. S5 *B* and *C*). Furthermore, even in the presence of ATP, pSae2 did not promote the exonuclease of MX in conjunction with the Rad50 KA variant that is not able to bind and hydrolyze ATP (Fig. 5 *G* and *H*). Thus, pSae2 promotes the exonuclease of MRX when ATP hydrolysis is allowed. The requirement of nucleotide cofactor for the stimulation of MRX by pSae2 in exonuclease assays was identical to that required for endonucleolytic cleavage of DNA substrates with streptavidin-blocked ends (*SI Appendix*, Fig. S5*D*) (33). Collectively, our data suggest that pSae2 stimulates both the exonuclease and the endonuclease of MR and MRX when Rad50 hydrolyzes ATP.

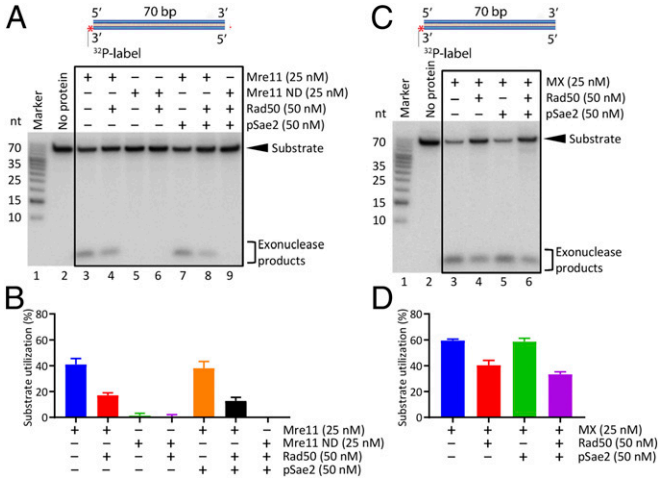

Fig. 4. The effects of Rad50·ATP and pSae2 on the cleavage of the terminal nucleotide at the 3′ end by Mre11. (*A*) A 3′-labeled 70-bp dsDNA substrate, with a 1-nt 3′ overhang created by terminal deoxynucleotidyl transferase, was incubated with Mre11, nuclease-dead Mre11 125–126 HD-LV (Mre11 ND), Rad50, and pSae2, as indicated. The reaction buffer contained ATP, 5 mM Mg^{2+}, and 1 mM Mn^{2+}. (*B*) Quantitation of experiments such as in *A*. $n = 3$. Error bars represent SEM. (*C*) Degradation of a 3′-labeled dsDNA substrate by MX, Rad50, and pSae2, as indicated. The reaction buffer contained ATP, 5 mM Mg^{2+}, and 1 mM Mn^{2+}. (*D*) Quantitation of experiments such as in *C*. $n = 3$. Error bars represent SEM.

The Rad50S Mutant Is Refractory to the Regulatory Control by Sae2. Alani et al. (40) identified separation of function *rad50* alleles (*rad50S*) that in contrast to *rad50*Δ, confer lower sensitivity to DNA-damaging drugs, but similarly to *rad50*Δ, block the resection of meiotic Spo11-bound DNA breaks. We previously reported that the Rad50 K81I variant (Rad50 KI, a Rad50S mutant) fails to clip dsDNA near protein-blocked DNA ends (33, 40) and fails to physically interact with pSae2 (36, 41, 42). We show here that Rad50 KI in complex with ATP also inhibited the exonuclease of Mre11, although not to the same extent as wild-type Rad50 (Figs. 2*B* and 6). However, in contrast to wild-type Rad50, pSae2 did not notably promote the exonuclease of Mre11-Rad50 KI·ATP (Fig. 6). Therefore, the Rad50 KI mutant is largely refractory to the regulatory control by pSae2, in agreement with a defect in its physical interaction with pSae2 (36).

Discussion

In the absence of the long-range DNA end resection pathways in vivo, the short-range resection catalyzed by MRX and Sae2 can degrade the 5′-terminated DNA strand up to ∼300 nt away from the end, while the 3′ end is largely, but not completely, protected (13, 26, 43, 44). Here we reconstituted the short-range resection with purified recombinant proteins. Using plasmid-length DNA substrates, we showed that the MRX-pSae2 ensemble resects blunt-ended DNA with a striking preference toward the 5′-terminated DNA strand, without any requirement for an additional protein block. Our experiments support a model in which multiple MRX-pSae2 complexes likely resect the 5′-terminated strand by stepwise incisions (Fig. 7*A*). The endonucleolytic cuts are followed by exonucleolytic degradation of the short fragments between the incision sites. In this model, one MRX-pSae2 unit directs DNA cleavage by the adjacent complex and in this way fulfills the requirement for a "protein block" identified in our previous work (33). MRX oligomerization at DSBs would also explain why the complex forms foci readily detectable

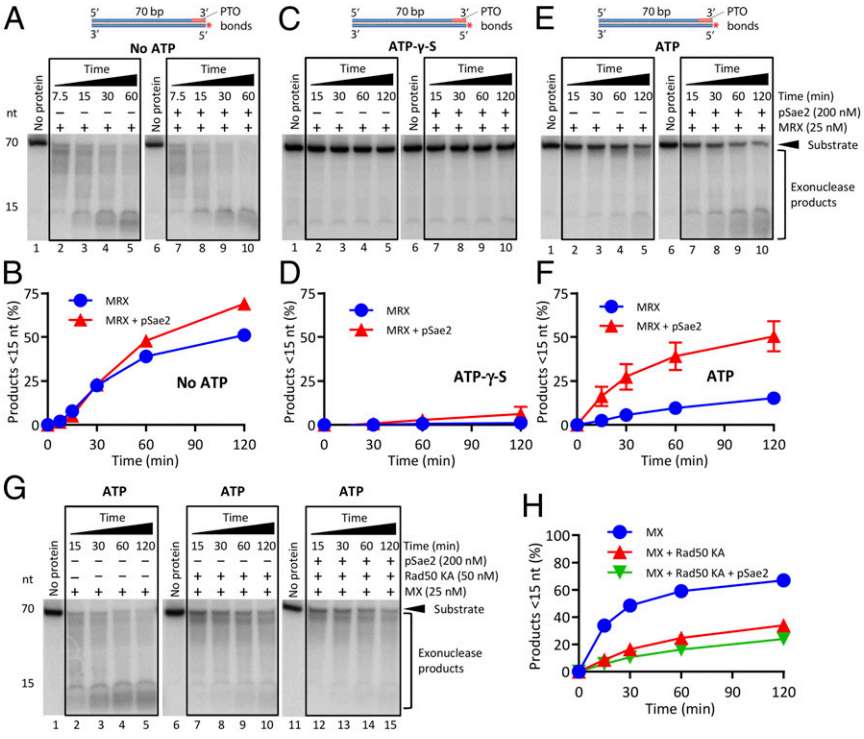

Fig. 5. The stimulation of Mre11 exonuclease by pSae2 requires ATP hydrolysis by Rad50. (*A*) Kinetics of DNA degradation by MRX without or with pSae2. The reaction buffer contained 5 mM Mg^{2+} and 1 mM Mn^{2+}, but no ATP. (*B*) Quantitation of experiments such as in *A*. $n \geq 3$. Error bars represent SEM. (*C*) Experiments such as in *A*, but with ATP-γ-S. (*D*) Quantitation of experiments such as in *C*. $n \geq 3$. Error bars represent SEM. (*E*) Experiments as in *A*, but with ATP. (*F*) Quantitation of experiments such as in *E*. $n \geq 3$. Error bars represent SEM. (*G*) Kinetics of DNA degradation by MX, ATP-binding–impaired Rad50 K40A (Rad50 KA), and pSae2, as indicated. The reaction buffer contained ATP, 5 mM Mg^{2+}, and 1 mM Mn^{2+}. (*H*) Quantitation of experiments such as in *G*. $n = 3$. Error bars represent SEM.

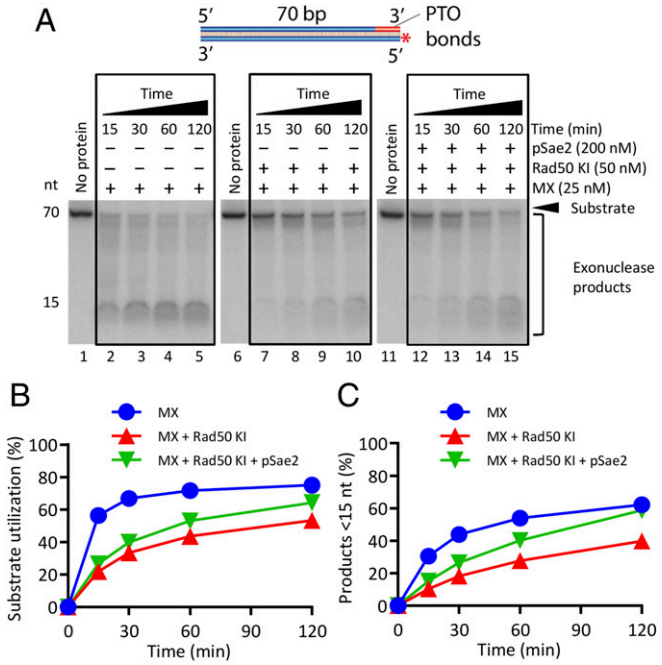

Fig. 6. The Rad50S mutant is refractory to the regulatory control by pSae2. (*A*) A kinetic assay showing the degradation of 5′-labeled dsDNA by MX, Rad50 K81I (Rad50 KI, corresponding to Rad50S), and pSae2. The reaction buffer contained ATP, 5 mM Mg^{2+}, and 1 mM Mn^{2+}. (*B*) Quantitation of overall substrate utilization from assays such as shown in *A*. $n = 3$. Error bars represent SEM. (*C*) Quantitation of products <15 nt from assays such as shown in *A*. $n = 3$. Error bars represent SEM.

by fluorescence microscopy (45). Finally, multiple DSB-bound MRX complexes can serve as a platform to amplify DNA damage signaling via ATM/Tel1, as even a single unrepaired DSB causes a cell cycle arrest (46).

In meiotic cells, it has been previously observed that a fraction of the Spo11 transesterase was initially bound to DNA fragments up to ∼300 nt long, which decreased in length over time (28). This observation suggests that MRX-pSae2 may first cleave DNA at a position distant from the DNA break (Fig. 7*B*); however, the 3′ end must be protected from the 3′→5′ exonucleolytic degradation by MRX (13). Spo11 in meiotic cells may have such a function (despite binding to the 5′ end), while Ku can protect the end in vegetative cells (17, 18). However, Ku is not an obligate component of the recombination machinery and thus is unlikely to be required to direct DNA cleavage by MRX-pSae2. In the stepwise resection model (Fig. 7*A*), the MRX and/or pSae2 complex might remain bound to the DNA end on endonucleolytic cleavage to protect it from exonucleolytic degradation by other MRX complexes. Likewise, the generation of a 3′ overhang would render it unsuitable for degradation by the MRX exonuclease, explaining why a separate protein block is not needed, particularly in vegetative cells. However, our data do not exclude the possibility that the distant-first cleavage (Fig. 7*B*) occurs in a fraction of cases, particularly in meiotic cells, where the architecture of the region surrounding Spo11 cleavage sites is tightly controlled, which might provide a signal for distant endonucleolytic DNA cleavage (47). Accordingly, the MRX-pSae2 ensemble can cleave next to internal protein blocks, such as nucleosomes (18). The resection end points correlated with nucleosome positions in Mre11-dependent resection in yeast cells (26). However, whether nucleosomes served as entry points for Mre11 or represented termination sites could not be distinguished (26).

It also remains to be established how DNA near internal protein blocks is cleaved to guarantee the 5′-specific strand degradation. To this point, it is possible that two MRX complexes may be separated by a DNA loop, which could explain the distant-first cleavage (Fig. 7*C*). Alternatively, the MRX complex could slide along dsDNA, providing such a signal. Indeed, the MRN complex was observed to diffuse along dsDNA in single molecule assays and to move past nucleosomes (48). While it appears that nucleosomes must be cleared or remodeled to allow long-range resection (49–51), more research is needed to define the interplay of MRX and pSae2 with chromatin.

We have shown here that under physiological conditions, when Mre11 is in complex with Rad50, the 3′→5′ exonuclease of Mre11 is restricted. The inhibition requires ATP binding, but not ATP hydrolysis by Rad50. This result may explain why the 3′→5′ exonuclease activity of Mre11 does not notably resect 3′-terminated strands at DSB sites in vivo (13). The inhibition of the Mre11 exonuclease by Rad50 is relieved by pSae2, which involves ATP hydrolysis by Rad50. As pSae2 at the same time also stimulates the endonucleolytic DNA cleavage by MRX (33), these reactions likely compete with each other. Our data demonstrate that the 5′-end degradation that involves endonucleolytic cleavage is clearly preferred when blunt-ended DNA is used.

The stimulation of both the exonuclease and the endonuclease of MRX by pSae2 is dependent on ATP hydrolysis by Rad50. Therefore, we hypothesized that pSae2 might control the Mre11 nuclease indirectly by regulating ATP hydrolysis by Rad50. However, we note that we failed to detect a direct effect of pSae2 on ATP hydrolysis by MR or MRX complex in ATPase assays. Because MRX hydrolyzes ATP nonproductively, we believe that the productive ATP hydrolysis that facilitates DNA degradation by the MR or MRX complex might represent only a small proportion of the total ATP hydrolyzed by Rad50 and thus was undetectable in our attempts. Alternatively, pSae2 may help couple ATP hydrolysis by MRX with DNA degradation by Mre11 without notably affecting the overall rate of ATP hydrolysis.

Several structural studies have demonstrated that the MR complex undergoes dramatic structural changes on ATP binding and hydrolysis by Rad50, which extend into the Mre11 nuclease active site (52–55). These transitions were proposed to regulate the balance between MR functions in NHEJ and signaling, which

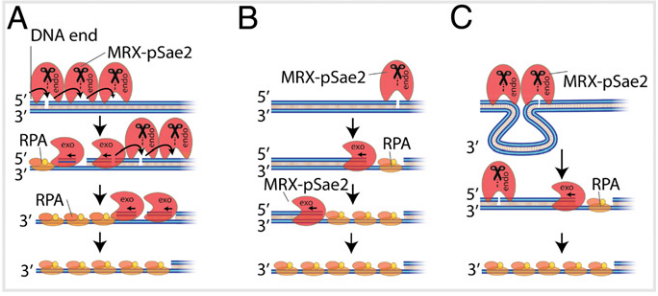

Fig. 7. Models for short-range DNA end resection by MRX-pSae2. (*A*) Data presented in this work support a model in which the MRX complex, in a reaction stimulated by pSae2, degrades the 5′-terminated DNA strand by stepwise endonucleolytic incisions. In this model, one MRX-pSae2 complex promotes cleavage by another complex that binds DNA at an adjacent site. The endonucleolytic cleavage is followed by exonucleolytic degradation of the DNA fragments between the incision sites in a 3′→5′ direction. Degradation of the 5′ strand protects the 3′ end from 3′→5′ exonuclease of MRX. (*B*) Data from yeast meiotic cells suggest that the first endonucleotic DNA cleavage occurs further away from the end (28). (*C*) A model that is a combination of *A* and *B*. One MRX-pSae2 complex may direct 5′ strand cleavage by another complex that binds DNA further away from the end. Details are provided in the text.

require ATP binding, unlike those in resection and HR, which require ATP hydrolysis. In archaea that lack Sae2/CtIP, these ATP-dependent conformation changes likely occur without a dedicated protein cofactor (52, 54, 55). We propose that pSae2/CtIP might represent a part of this switching mechanism in eukaryotic cells. This hypothesis is further supported by our previous observation that phosphorylation of Sae2 promotes its physical interaction with Rad50 (36). However, the exact mechanism of how pSae2 and Rad50 ATPase functions integrate to regulate Mre11 remains to be demonstrated directly.

In summary, our results suggest that Rad50 and pSae2 turn Mre11, a 3′ → 5′ exonuclease, into a molecular machine that preferentially degrades 5′-terminated DNA strands at DSB sites in a stepwise manner. We believe this mode of DNA degradation can help overcome any obstacles present not only at DNA ends, but also at sites internal to the DSBs. This short-range DNA degradation in turn facilitates the long-range resection pathways acting downstream to promote HR.

Materials and Methods

Preparation of Recombinant Proteins. All proteins were expressed in *Spodoptera frugiperda* 9 (*Sf*9) cells according to standard procedures. Unless indicated otherwise, frozen pellets of infected *Sf*9 cells were resuspended at 4 °C in extraction buffer containing 50 mM Tris·HCl pH 7.5, 5 mM β-mercaptoethanol, 1 mM EDTA, 1 mM phenylmethylsulfonyl fluoride (PMSF), 30 μg/mL leupeptin, and protease inhibitor mixture (P8340, 1:400; Sigma-Aldrich). The suspension was incubated for 20 min with gentle agitation. Then one-half volume of 50% glycerol was added, followed by 6.5% volume of 5 M NaCl (final concentration 325 mM). The proteins were extracted during a 30-min incubation with gentle agitation. The soluble extract was obtained on centrifugation at 55,000 × *g* for 30 min.

Recombinant Mre11 was obtained using pFB-MBP-Mre11-His vector coding for Mre11-His. The soluble extract was bound to amylose resin (New England BioLabs), followed by extensive washing with wash buffer containing 50 mM Tris·HCl pH 7.5, 5 mM β-mercaptoethanol, 1 M NaCl, 1 mM PMSF, and 10% (vol/vol) glycerol. Mre11 was eluted with elution buffer containing 50 mM Tris·HCl pH 7.5, 5 mM β-mercaptoethanol, 300 mM NaCl, 1 mM PMSF, 10% (vol/vol) glycerol, and 10 mM maltose. The MBP tag was cleaved with PreScission protease for 2 h at 4 °C. Imidazole was added to a final concentration of 10 mM, and Mre11 was bound to NiNTA resin (Qiagen). The resin was washed with buffer A1 containing 50 mM Tris·HCl pH 7.5, 5 mM β-mercaptoethanol, 1 M NaCl, 0.5 mM PMSF, 10% (vol/vol) glycerol, and 40 mM imidazole. Then the resin was washed with buffer A2 containing 50 mM Tris·HCl pH 7.5, 5 mM β-mercaptoethanol, 150 mM NaCl, 0.5 mM PMSF, 10% (vol/vol) glycerol and 58 mM imidazole. The proteins were eluted with buffer B containing 50 mM Tris·HCl pH 7.5, 5 mM β-mercaptoethanol, 150 mM NaCl, 0.5 mM PMSF, 10% (vol/vol) glycerol, and 300 mM imidazole. Mre11 125–126 HD-LV mutant (Mre11 ND) was prepared in an identical way. The yield was ∼0.5 mg Mre11 from 400 mL of *Sf*9 cells.

Recombinant Xrs2-FLAG was prepared using pTP694 vector (a gift from T. Paull). The soluble extract was prepared with an extraction buffer containing only 0.5 mM β-mercaptoethanol and no EDTA. The soluble extract was then incubated with anti-FLAG M2 affinity resin (Sigma-Aldrich). The resin was first washed with wash buffer 1 containing 50 mM Tris·HCl pH 7.5, 0.5 mM β-mercaptoethanol, 300 mM NaCl, 0.5 mM PMSF, 10% (vol/vol) glycerol, and 0.1% (vol/vol) Nonidet P-40. The washing was very extensive (1.5 h, ∼150 mL of buffer per 0.5 mL resin). The resin was then extensively washed with wash buffer 2 containing 50 mM Tris·HCl pH 7.5, 0.5 mM β-mercaptoethanol, 150 mM NaCl, 0.5 mM PMSF, and 10% (vol/vol) glycerol. Xrs2 was eluted with wash buffer 2 supplemented with 200 μg/mL 3× FLAG peptide (Sigma-Aldrich). The yield was ∼50 μg from 400 mL of *Sf*9 cells. Recombinant wild-type Rad50-FLAG and mutants were prepared similarly using pFB-Rad50-FLAG vector and its variants. The yield was ∼100 μg from 800 mL of *Sf*9 cells.

The MR complex was prepared using vectors coding for Mre11-his (pTP391 provided by T. Paull) and untagged Rad50 (pFB-Rad50) as described previously (56). In brief, the proteins were coexpressed in *Sf*9 cells, and the soluble extract was incubated with NiNTA resin. The MR complex was then further purified on HiTrap Q and HiTrap S ion exchange chromatography columns. The MX and MRX complexes were purified by coexpression in *Sf*9 cells using vectors coding for Mre11-His, Rad50, and Xrs2-FLAG, as described previously (33, 57).

pSae2 was prepared as described previously in the presence of phosphatase inhibitors (36). The λ phosphatase treatment was carried out as described previously (36). The pSae2 S267A and S267E variants were prepared in the same way as wild-type pSae2 in the presence of phosphatase inhibitors. Yeast RPA was expressed in *E. coli* from p11d-scRPA vector (a kind gift from M. Wold, University of Iowa) and purified as described for human recombinant RPA (58).

DNA Substrate Preparation. To prepare the 5′-labeled 70-bp-long dsDNA substrate, the bottom-strand PC217 was first labeled with [γ-^{32}P]ATP (PerkinElmer) and T4 polynucleotide kinase (New England BioLabs) according to the manufacturer's instructions. (The oligonucleotides used in this study are listed in *SI Appendix*, Table S1.) The reaction was terminated and purified twice on a G25 column (GE Healthcare). The labeled bottom strand was then annealed with twofold excess of the unlabeled top strand PC216_5XSS in 1× T4 polynucleotide kinase buffer (New England BioLabs). The 3′-labeled substrate was prepared similarly, except the bottom DNA strand was labeled with [α-^{32}P] cordycepin 5′-triphosphate (PerkinElmer) and terminal transferase (New England BioLabs). The streptavidin-blocked 70-bp-long DNA substrate was prepared as described previously with oligonucleotides 210 and 211 (33). Internal thymidine (**T**, in bold) contained a biotin label where indicated.

The 5′ overhanged 2.7-kbp-long DNA substrate was prepared by the digestion of the pOH-S vector by StuI (New England BioLabs), followed by Nb. BbvC1 (New England BioLabs) and partial heat denaturation, as described previously (59). The blunt-ended 2.8-kbp-long DNA substrates without or with biotin labels at the end, as indicated, were prepared as described previously using pAttP-S vectors, annealed oligonucleotides (210 and 211 for all experiments except Fig. 1*I*), and ΦC31 integrase (59). The oligonucleotides used for preparation of the 2.8-kbp-long substrate used in Fig. 1*I* were PC206 and 209 (33). PCR was used to generate the 1.7- and 1.0-kbp substrates in Fig. 1*I*. Primers PL_for and PL_rev-1000 were used for preparation of the 1.0-kbp substrate and PL_for and PL_rev-1700 primers for the 1.7-kbp substrate.

The randomly labeled 2.2-kbp-long DNA substrate was prepared by PCR-based amplification using the pFB-MBP-NBS1-His vector as template and primers NBS1_F and NBS1_R. The PCR was carried out under standard conditions, and supplemented with 1 μM [α-^{32}P] dCTP (PerkinElmer) on top of the 200 μM cold dCTP. The PCR product was purified first with a PCR purification kit (Qiagen) and subsequently with Chroma Spin G400 column (Clontech). The final concentration of the labeled DNA was estimated by comparing labeled DNA with various dilutions of unlabeled DNA of a known concentration. The DNA samples were separated by agarose gel electrophoresis and stained with GelRed.

Nuclease Assays. Unless indicated otherwise, the assays were carried out in a 15-μL reaction volume. The reaction buffer contained 25 mM Tris-acetate pH 7.5, 1 mM DTT, 0.25 mg/mL BSA (New England BioLabs), 1 nM (in molecules) DNA substrate (both oligonucleotide-based and plasmid-length, unless indicated otherwise), and indicated concentrations of Mn^{2+} and Mg^{2+}. All reactions with plasmid-length DNA substrates contained 5 mM Mg^{2+} and 1 mM Mn^{2+}. As described, the reactions were further supplemented with 1 mM of ATP (GE Healthcare), ATP-γ-S (Cayman Chemical Company), ADP (Alfa Aesar), AMP-PNP (Sigma-Aldrich), or sodium orthovanadate (Vi; Sigma-Aldrich) or contained no additional cofactor. Unless indicated otherwise, reactions with ATP also contained an ATP regeneration system that included 80 U/mL pyruvate kinase (Sigma-Aldrich) and 1 mM phosphoenolpyruvate (Sigma-Aldrich).

The reactions were assembled on ice, and recombinant proteins (as indicated) were added last. The assays were carried out at 30 °C for 30 min unless indicated otherwise. The reactions were terminated with 0.5 μL of 0.5 M EDTA, 0.5 μL of 10% SDS, and 0.5 μL of proteinase K (14–22 mg/mL; Roche), followed by a 30-min incubation at 50 °C. Terminated reactions with oligonucleotide-based DNA were then mixed with an equal volume of loading dye (95% formamide, 20 mM EDTA, and 1 mg/mL bromophenol blue). Then 15 μL of the sample from each reaction was separated by denaturing polyacrylamide electrophoresis as described previously (59). A 5′-labeled low molecular weight marker (J76410; Affymetrix) was used where indicated. The gels were dried on 3MM paper (Whatman), exposed to storage phosphor screens, and analyzed using a Typhoon imager (GE Healthcare). The data were quantitated using ImageJ.

Degradation of the substrate (indicated as substrate utilization) was determined by calculating the percentage of unreacted substrate compared with a control lane (100%). We note that due to the resolution of the gel, this analysis might miss substrate shortening by 1–2 nt. Degradation products smaller than 15 nt (products <15 nt) were quantitated as a percentage of these small fragments compared with the total signal in the respective lanes.

The nuclease assays (15 μL volume) with plasmid-length DNA substrates were terminated with 5 μL of STOP buffer (30 mM EDTA, 2% SDS, 30%

glycerol, and 1 mg/mL bromophenol blue) and 1 μL of proteinase K (14–22 mg/mL; Roche) for 30 min at 37 °C. Magnesium acetate was then added to a final concentration 10 mM (free final magnesium concentration, 7.5 mM) to facilitate subsequent DNA annealing. The reactions were then mixed with one of five oligonucleotides ^{32}P-labeled at the 5′ end— 3′_OligoA, 5′_OligoA, 5′_OligoB, 5′_OligoC, or 3′_OligoD—using a threefold excess over the DNA substrate (3 nM final concentration). The oligonucleotides of the "A" series, 3′_OligoA and 5′_OligoA, anneal 100 nt away from the DNA end of the 2.7-kbp-long substrate and 160 nt away from the DNA end of the 2.8-, 1.7-, and 1-kbp-long substrates, respectively (*SI Appendix*, Table S1). In all cases, the underscored sequences are complementary to the substrate DNA; the GG overhangs were included to facilitate comparable labeling.

The samples were heated to 60 °C for 5 min, and the annealing occurred during a gradual cooling overnight. The samples were then separated by electrophoresis in 1% agarose in TAE buffer (40 mM Tris, 20 mM acetate, and 1 mM EDTA). The gels were dried on DE81 paper (Whatman) and processed as described above. Degradation of the substrate was quantitated as a percentage of annealed oligonucleotide over the total signal in the lane, corrected for the excess of oligonucleotide used for annealing.

ACKNOWLEDGMENTS. We thank members of the P.C. laboratory for discussions and comments on the manuscript. This work was supported by the Swiss National Science Foundation (Grant 31003A_175444, to P.C.) and European Research Council (Grant 681630, to P.C.).

1. Ciccia A, Elledge SJ (2010) The DNA damage response: Making it safe to play with knives. *Mol Cell* 40:179–204.
2. Ranjha L, Howard SM, Cejka P (2018) Main steps in DNA double-strand break repair: An introduction to homologous recombination and related processes. *Chromosoma* 127:187–214.
3. Chang HHY, Pannunzio NR, Adachi N, Lieber MR (2017) Non-homologous DNA end joining and alternative pathways to double-strand break repair. *Nat Rev Mol Cell Biol* 18:495–506.
4. Kowalczykowski SC (2015) An overview of the molecular mechanisms of recombinational DNA repair. *Cold Spring Harb Perspect Biol* 7:a016410.
5. Cejka P (2015) DNA end resection: Nucleases team up with the right partners to initiate homologous recombination. *J Biol Chem* 290:22931–22938.
6. Chen L, Trujillo K, Ramos W, Sung P, Tomkinson AE (2001) Promotion of Dnl4-catalyzed DNA end-joining by the Rad50/Mre11/Xrs2 and Hdf1/Hdf2 complexes. *Mol Cell* 8:1105–1115.
7. Lee JH, Paull TT (2004) Direct activation of the ATM protein kinase by the Mre11/Rad50/Nbs1 complex. *Science* 304:93–96.
8. Paull TT, Gellert M (2000) A mechanistic basis for Mre11-directed DNA joining at microhomologies. *Proc Natl Acad Sci USA* 97:6409–6414.
9. de Jager M, et al. (2001) Human Rad50/Mre11 is a flexible complex that can tether DNA ends. *Mol Cell* 8:1129–1135.
10. Johzuka K, Ogawa H (1995) Interaction of Mre11 and Rad50: Two proteins required for DNA repair and meiosis-specific double-strand break formation in *Saccharomyces cerevisiae*. *Genetics* 139:1521–1532.
11. Trujillo KM, Sung P (2001) DNA structure-specific nuclease activities in the *Saccharomyces cerevisiae* Rad50*Mre11 complex. *J Biol Chem* 276:35458–35464.
12. Paull TT, Gellert M (1998) The 3′ to 5′ exonuclease activity of Mre 11 facilitates repair of DNA double-strand breaks. *Mol Cell* 1:969–979.
13. Zhu Z, Chung WH, Shim EY, Lee SE, Ira G (2008) Sgs1 helicase and two nucleases Dna2 and Exo1 resect DNA double-strand break ends. *Cell* 134:981–994.
14. Mimitou EP, Symington LS (2008) Sae2, Exo1 and Sgs1 collaborate in DNA double-strand break processing. *Nature* 455:770–774.
15. Cejka P, et al. (2010) DNA end resection by Dna2-Sgs1-RPA and its stimulation by Top3-Rmi1 and Mre11-Rad50-Xrs2. *Nature* 467:112–116.
16. Niu H, et al. (2010) Mechanism of the ATP-dependent DNA end-resection machinery from *Saccharomyces cerevisiae*. *Nature* 467:108–111.
17. Reginato G, Cannavo E, Cejka P (2017) Physiological protein blocks direct the Mre11-Rad50-Xrs2 and Sae2 nuclease complex to initiate DNA end resection. *Genes Dev* 31:2325–2330.
18. Wang W, Daley JM, Kwon Y, Krasner DS, Sung P (2017) Plasticity of the Mre11-Rad50-Xrs2-Sae2 nuclease ensemble in the processing of DNA-bound obstacles. *Genes Dev* 31:2331–2336.
19. Llorente B, Symington LS (2004) The Mre11 nuclease is not required for 5′ to 3′ resection at multiple HO-induced double-strand breaks. *Mol Cell Biol* 24:9682–9694.
20. Mimitou EP, Symington LS (2010) Ku prevents Exo1 and Sgs1-dependent resection of DNA ends in the absence of a functional MRX complex or Sae2. *EMBO J* 29:3358–3369.
21. Neale MJ, Pan J, Keeney S (2005) Endonucleolytic processing of covalent protein-linked DNA double-strand breaks. *Nature* 436:1053–1057.
22. Lobachev KS, Gordenin DA, Resnick MA (2002) The Mre11 complex is required for repair of hairpin-capped double-strand breaks and prevention of chromosome rearrangements. *Cell* 108:183–193.
23. Shibata A, et al. (2014) DNA double-strand break repair pathway choice is directed by distinct MRE11 nuclease activities. *Mol Cell* 53:7–18.
24. Langerak P, Mejia-Ramirez E, Limbo O, Russell P (2011) Release of Ku and MRN from DNA ends by Mre11 nuclease activity and Ctp1 is required for homologous recombination repair of double-strand breaks. *PLoS Genet* 7:e1002271.
25. Trujillo KM, Yuan SS, Lee EY, Sung P (1998) Nuclease activities in a complex of human recombination and DNA repair factors Rad50, Mre11, and p95. *J Biol Chem* 273:21447–21450.
26. Mimitou EP, Yamada S, Keeney S (2017) A global view of meiotic double-strand break end resection. *Science* 355:40–45.
27. Keeney S, Kleckner N (1995) Covalent protein-DNA complexes at the 5′ strand termini of meiosis-specific double-strand breaks in yeast. *Proc Natl Acad Sci USA* 92:11274–11278.
28. Garcia V, Phelps SE, Gray S, Neale MJ (2011) Bidirectional resection of DNA double-strand breaks by Mre11 and Exo1. *Nature* 479:241–244.
29. Foster SS, Balestrini A, Petrini JH (2011) Functional interplay of the Mre11 nuclease and Ku in the response to replication-associated DNA damage. *Mol Cell Biol* 31:4379–4389.
30. Clerici M, Mantiero D, Guerini I, Lucchini G, Longhese MP (2008) The Yku70-Yku80 complex contributes to regulate double-strand break processing and checkpoint activation during the cell cycle. *EMBO Rep* 9:810–818.
31. Bonetti D, Clerici M, Manfrini N, Lucchini G, Longhese MP (2010) The MRX complex plays multiple functions in resection of Yku- and Rif2-protected DNA ends. *PLoS One* 5:e14142.
32. Anand R, Ranjha L, Cannavo E, Cejka P (2016) Phosphorylated CtIP functions as a co-factor of the MRE11-RAD50-NBS1 endonuclease in DNA end resection. *Mol Cell* 64:940–950.
33. Cannavo E, Cejka P (2014) Sae2 promotes dsDNA endonuclease activity within Mre11-Rad50-Xrs2 to resect DNA breaks. *Nature* 514:122–125.
34. Deshpande RA, Lee JH, Arora S, Paull TT (2016) Nbs1 converts the human Mre11/Rad50 nuclease complex into an endo/exonuclease machine specific for protein-DNA adducts. *Mol Cell* 64:593–606.
35. Chen L, et al. (2005) Effect of amino acid substitutions in the rad50 ATP binding domain on DNA double-strand break repair in yeast. *J Biol Chem* 280:2620–2627.
36. Cannavo E, et al. (2018) Regulatory control of DNA end resection by Sae2 phosphorylation. *Nat Commun* 9:4016.
37. Bressan DA, Olivares HA, Nelms BE, Petrini JH (1998) Alteration of N-terminal phosphoesterase signature motifs inactivates *Saccharomyces cerevisiae* Mre11. *Genetics* 150:591–600.
38. Oldham ML, Chen J (2011) Snapshots of the maltose transporter during ATP hydrolysis. *Proc Natl Acad Sci USA* 108:15152–15156.
39. Huertas P, Cortés-Ledesma F, Sartori AA, Aguilera A, Jackson SP (2008) CDK targets Sae2 to control DNA-end resection and homologous recombination. *Nature* 455:689–692.
40. Alani E, Padmore R, Kleckner N (1990) Analysis of wild-type and rad50 mutants of yeast suggests an intimate relationship between meiotic chromosome synapsis and recombination. *Cell* 61:419–436.
41. Clerici M, Mantiero D, Lucchini G, Longhese MP (2005) The *Saccharomyces cerevisiae* Sae2 protein promotes resection and bridging of double-strand break ends. *J Biol Chem* 280:38631–38638.
42. Hopfner KP, et al. (2001) Structural biochemistry and interaction architecture of the DNA double-strand break repair Mre11 nuclease and Rad50-ATPase. *Cell* 105:473–485.
43. Pâques F, Haber JE (1997) Two pathways for removal of nonhomologous DNA ends during double-strand break repair in *Saccharomyces cerevisiae*. *Mol Cell Biol* 17:6765–6771.
44. Zakharyevich K, et al. (2010) Temporally and biochemically distinct activities of Exo1 during meiosis: Double-strand break resection and resolution of double Holliday junctions. *Mol Cell* 40:1001–1015.
45. Usui T, et al. (1998) Complex formation and functional versatility of Mre11 of budding yeast in recombination. *Cell* 95:705–716.
46. Sandell LL, Zakian VA (1993) Loss of a yeast telomere: Arrest, recovery, and chromosome loss. *Cell* 75:729–739.
47. Lam I, Keeney S (2014) Mechanism and regulation of meiotic recombination initiation. *Cold Spring Harb Perspect Biol* 7:a016634.
48. Myler LR, et al. (2017) Single-molecule imaging reveals how Mre11-Rad50-Nbs1 initiates DNA break repair. *Mol Cell* 67:891–898.e4.
49. Adkins NL, Niu H, Sung P, Peterson CL (2013) Nucleosome dynamics regulates DNA processing. *Nat Struct Mol Biol* 20:836–842.
50. Chen X, et al. (2012) The Fun30 nucleosome remodeller promotes resection of DNA double-strand break ends. *Nature* 489:576–580.
51. Costelloe T, et al. (2012) The yeast Fun30 and human SMARCAD1 chromatin remodellers promote DNA end resection. *Nature* 489:581–584.
52. Deshpande RA, et al. (2014) ATP-driven Rad50 conformations regulate DNA tethering, end resection, and ATM checkpoint signaling. *EMBO J* 33:482–500.
53. Lammens K, et al. (2011) The Mre11:Rad50 structure shows an ATP-dependent molecular clamp in DNA double-strand break repair. *Cell* 145:54–66.
54. Liu Y, et al. (2016) ATP-dependent DNA binding, unwinding, and resection by the Mre11/Rad50 complex. *EMBO J* 35:743–758.
55. Majka J, Alford B, Ausio J, Finn RM, McMurray CT (2012) ATP hydrolysis by RAD50 protein switches MRE11 enzyme from endonuclease to exonuclease. *J Biol Chem* 287:2328–2341.
56. Oh J, Al-Zain A, Cannavo E, Cejka P, Symington LS (2016) Xrs2 dependent and independent functions of the Mre11-Rad50 complex. *Mol Cell* 64:405–415.
57. Cannavo E, Cejka P, Kowalczykowski SC (2013) Relationship of DNA degradation by *Saccharomyces cerevisiae* exonuclease 1 and its stimulation by RPA and Mre11-Rad50-Xrs2 to DNA end resection. *Proc Natl Acad Sci USA* 110:E1661–E1668.
58. Anand R, Pinto C, Cejka P (2018) Methods to study DNA end resection, I: Recombinant protein purification. *Methods Enzymol* 600:25–66.
59. Pinto C, Anand R, Cejka P (2018) Methods to study DNA end resection, II: Biochemical reconstitution assays. *Methods Enzymol* 600:67–106.